



# Performance of the Muon Identification at LHCb

The LHCb MuonID group <sup>†</sup>

## Abstract

The performance of the muon identification in LHCb is extracted from data using muons and hadrons produced in  $J/\psi \rightarrow \mu^+\mu^-$ ,  $\Lambda^0 \rightarrow p\pi^-$  and  $D^{*+} \rightarrow \pi^+D^0(K^-\pi^+)$  decays. The muon identification procedure is based on the pattern of hits in the muon chambers. A momentum dependent binary requirement is used to reduce the probability of hadrons to be misidentified as muons to the level of 1%, keeping the muon efficiency in the range of 95-98%. As further refinement, a likelihood is built for the muon and non-muon hypotheses. Adding a requirement on this likelihood that provides a total muon efficiency at the level of 93%, the hadron misidentification probabilities are below 0.6%.

(To be submitted to JINST)

---

<sup>†</sup>Authors are listed on the following pages.



## The LHCb MuonID Group

F. Archilli<sup>1</sup>, W. Baldini<sup>2</sup>, G. Bencivenni<sup>1</sup>, N. Bondar<sup>3</sup>, W. Bonivento<sup>4</sup>, S. Cadeddu<sup>4</sup>, P. Campana<sup>1</sup>, A. Cardini<sup>4</sup>, M. Carletti<sup>1</sup>, P. Ciambrone<sup>1</sup>, X. Cid Vidal<sup>5</sup>, C. Deplano<sup>4</sup>, P. De Simone<sup>1</sup>, M. Frosini<sup>6</sup>, S. Furcas<sup>1,a</sup>, E. Furfaro<sup>7</sup>, M. Gandelman<sup>8</sup>, J.A. Hernando Morata<sup>9</sup>, G. Graziani<sup>6</sup>, A. Lai<sup>4</sup>, G. Lanfranchi<sup>1</sup>, J.H. Lopes<sup>8</sup>, O. Maev<sup>3</sup>, G. Manca<sup>4</sup>, G. Martellotti<sup>7</sup>, A. Massafferri<sup>10</sup>, D. Milanese<sup>11</sup>, R. Oldeman<sup>4,13</sup>, M. Palutan<sup>1</sup>, G. Passaleva<sup>6</sup>, D. Pinci<sup>7</sup>, E. Polycarpo<sup>8</sup>, R. Santacesaria<sup>7</sup>, E. Santovetti<sup>12,14</sup>, A. Sarti<sup>1,16</sup>, A. Satta<sup>12</sup>, B. Schmidt<sup>5</sup>, B. Sciascia<sup>1</sup>, F. Soomro<sup>1</sup>, A. Sciubba<sup>7,16</sup>, S. Vecchi<sup>2</sup>.

<sup>1</sup>*INFN - Laboratori Nazionali di Frascati, Italy*

<sup>2</sup>*Sezione INFN di Ferrara, Ferrara, Italy*

<sup>3</sup>*Petersburg Nuclear Physics Institute, Gatchina, St-Petersburg, Russia*

<sup>4</sup>*Sezione INFN di Cagliari, Cagliari, Italy*

<sup>5</sup>*European Organisation for Nuclear Research (CERN), Geneva, Switzerland*

<sup>6</sup>*Sezione INFN di Firenze, Firenze, Italy*

<sup>7</sup>*Sezione INFN di Roma, Roma, Italy* <sup>8</sup>*Instituto de Física, Universidade Federal do Rio de Janeiro (UFRJ), Brasil*

<sup>9</sup>*Universidade de Santiago de Compostela, Santiago de Compostela, Spain*

<sup>10</sup>*Centro Brasileiro de Pesquisas Físicas (CBPF), Rio de Janeiro, Brasil*

<sup>11</sup>*Sezione INFN di Bari, Bari, Italy*

<sup>12</sup>*Sezione INFN di Roma Tor Vergata, Roma, Italy*

<sup>13</sup>*Università di Cagliari, Cagliari, Italy*

<sup>14</sup>*Università di Firenze, Firenze, Italy*

<sup>15</sup>*Università di Roma Tor Vergata, Roma, Italy*

<sup>16</sup>*Sapienza, Università di Roma, Roma, Italy*

<sup>a</sup>*Now at Sezione INFN di Milano, Milano, Italy*

# Contents

<b>1</b>	<b>Introduction</b>	<b>1</b>
<b>2</b>	<b>The LHCb experiment and the muon system</b>	<b>1</b>
<b>3</b>	<b>The muon identification procedure</b>	<b>3</b>
3.1	IsMuon binary selection . . . . .	3
3.2	Muon and non-muon likelihoods . . . . .	4
3.3	Combined likelihoods . . . . .	5
3.4	Discriminating variable based on hits sharing . . . . .	6
<b>4</b>	<b>Method for the extraction of efficiencies</b>	<b>7</b>
4.1	Selection of control samples . . . . .	7
4.2	Efficiency evaluation . . . . .	8
<b>5</b>	<b>Results</b>	<b>8</b>
5.1	IsMuon performance . . . . .	8
5.2	Muon likelihoods . . . . .	12
5.3	Combined likelihoods . . . . .	12
5.4	NShared performance . . . . .	13
5.5	Systematic checks . . . . .	14
<b>6</b>	<b>Conclusions</b>	<b>16</b>

# 1 Introduction

LHCb [1] is a dedicated heavy flavour experiment, designed to exploit the high  $pp \rightarrow c\bar{c}$  and  $pp \rightarrow b\bar{b}$  cross-sections at the LHC in order to perform precision measurements of CP violation and rare decays. Muons are present in the final state of many of the key decays, sensitive to new physics, as shown, for example, in [2, 3, 4, 5, 6, 7, 8, 9]. Moreover, they play a crucial role in the determination of the flavor tagging of the neutral  $B$  mesons and are also present in the signatures of interesting electroweak and strong processes. The muon identification procedure must provide high muon efficiency while keeping the incorrect identification probability of hadrons as muons (misidentification probabilities) at the lowest possible level. The pion misidentification is one of the major sources of combinatoric background for decays with muons in the final state. It is also important to keep the other hadron misidentification probabilities at low levels so that rare decays can be separated from more abundant hadronic decays with similar or identical topology.

This paper presents the performance of the muon identification in LHCb, obtained from the data recorded in 2011, corresponding to approximately  $1 \text{ fb}^{-1}$ . In Section 2, a brief description of the LHCb spectrometer and the muon detection system is given. The muon identification algorithm is discussed in Section 3. The method used to extract the muon efficiency and the misidentification probability from data is explained in Section 4. Finally, the performance results are presented in Section 5, followed by the conclusions in Section 6.

## 2 The LHCb experiment and the muon system

The LHCb detector [1] is a single-arm forward spectrometer. A vertex locator (VELO) determines with high precision the positions of the vertices of  $pp$  collisions (PVs) and the decay vertices of long-lived particles. The tracking system includes a silicon strip detector located in front of a dipole magnet with an integrated field of about 4 Tm, and a combination of silicon strip detectors and straw drift chambers placed behind the magnet. The momentum of charged particles is determined with a resolution of  $\sigma_p/p \sim 0.4(0.6)\%$  at a momentum scale of  $3(100) \text{ GeV}/c$ . Charged hadron identification is achieved with two ring-imaging Cherenkov (RICH) detectors. The calorimeter system consists of a scintillator pad detector, a preshower, an electromagnetic calorimeter and a hadronic calorimeter. It identifies high transverse energy hadron, electron and photon candidates and provides information for the trigger.

The muon system [10] is composed of five stations (M1-M5) of rectangular shape, placed along the beam axis, as shown in Fig. 1. Station M1 is located in front of the calorimeters and is used to improve the transverse momentum measurement in the first level hardware trigger. Stations M2 to M5 are placed downstream the calorimeters and are interleaved with iron absorbers 80 cm thick to select penetrating muons. The total absorber thickness in front of station M2, including the calorimeters, is approximately 6.6 interaction lengths. More than 99% of the total area of the system is equipped with multi-wire proportional chambers (MWPC) with Ar/CO<sub>2</sub>/CF<sub>4</sub>(40:55:5) as gas mixture.

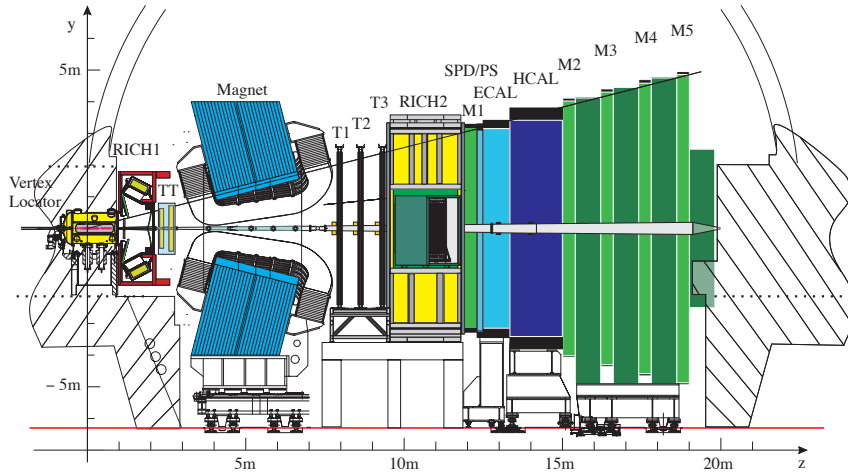


Figure 1: Schematic view of the LHCb experiment. The muon stations are seen as the five green vertical bars, the second one placed just after the calorimeters, shown as the blue rectangles.

41 Only the inner part of the first station is instrumented with triple-GEM detectors filled  
 42 with Ar/CO<sub>2</sub>/CF<sub>4</sub>(45:15:40).

43 The chambers are positioned to provide with their sensitive area a hermetic geometric  
 44 acceptance to high momentum particles coming from the interaction point. In addi-  
 45 tion, the chambers of different stations form projective towers pointing to the interac-  
 46 tion point. The detectors provide digital space point measurements of the particle trajectories,  
 47 supplying information to the trigger processor and to the data acquisition (DAQ). The  
 48 information is obtained by partitioning the detector into rectangular logical pads whose  
 49 dimensions define the x, y resolution in the plane perpendicular to the beam axis. Each  
 50 station is divided into four regions, R1 to R4 with increasing distance from the beam  
 51 axis, as shown in Fig. 2. The linear dimensions of the regions R1, R2, R3, R4, and their  
 52 segmentation scale in the ratio 1:2:4:8. Each muon station is designed to perform with an  
 53 efficiency above 99% in a 20 ns time window with a noise rate below 1 kHz per physical  
 54 channel, which was achieved during operation, as described in [10].

55 The muon system provides information for the selection of high transverse momentum  
 56 muons at the trigger level and for the offline muon identification. This document refers  
 57 to the latter procedure, which uses only the information from the 4 stations located after  
 58 the calorimeters. The muon identification in the trigger system is described in [11].

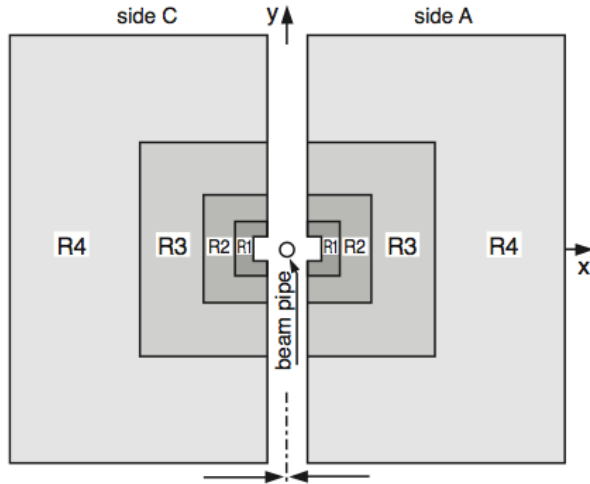


Figure 2: Schematic view of one muon system station (reproduced from [10]).

### 3 The muon identification procedure

The muon identification strategy can be divided in three steps:

- A loose binary selection of muon candidates based on the penetration of the muons through the calorimeters and iron filters, which provides high efficiency while reducing the misidentification probability of hadrons to the percent level (called IsMuon);
- Computation of a likelihood for the muon and non-muon hypotheses, based on the pattern of hits around the extrapolation to the different muon stations of the charged particles trajectories reconstructed with high precision in the tracking system. The logarithm of the ratio between the muon and non-muon hypotheses is used as discriminating variable and called muDLL.
- Computation of a combined likelihood for the different particle hypotheses, including information from the calorimeter and RICH systems. The logarithm of the ratio between the muon and pion hypotheses is used as discriminating variable and called DLL.

Additionally the number of tracks identified as muons that share a hit with a given muon candidate (called NShared) can be used to further reject false candidates.

#### 3.1 IsMuon binary selection

The binary selection is defined according to the number of stations where a hit is found within a field of interest (FOI) defined around the track extrapolation. The number of stations required to have a muon signal is a function of track momentum ( $p$ ), as shown in Table 1. The sizes of the fields of interest also depend on the particle momentum

and are defined according to the expected multiple scattering suffered by a muon when traversing the material. The FOI are parameterized separately for the 4 regions of the 4 different stations downstream the calorimeter in both  $x$  and  $y$  directions according to:

$$\text{FOI} = a + b \times \exp(-c \times p). \quad (1)$$

76 The parameters  $a$ ,  $b$  and  $c$  have been determined using muons from a full detector Monte  
77 Carlo simulation [12].

Momentum range	Muon stations
$3 \text{ GeV}/c < p < 6 \text{ GeV}/c$	M2 and M3
$6 \text{ GeV}/c < p < 10 \text{ GeV}/c$	M2 and M3 and (M4 or M5)
$p > 10 \text{ GeV}/c$	M2 and M3 and M4 and M5

Table 1: Muon stations required to trigger the IsMuon decision as a function of momentum range.

78 For tracks passing the IsMuon requirement, the muon identification can be further  
79 improved by a selection based on the logarithm of the ratio between the likelihoods for  
80 the muon and non-muon hypotheses (muDLL).

### 81 3.2 Muon and non-muon likelihoods

82 The likelihoods are computed as the cumulative probability distributions of the average  
83 squared distance significance  $D^2$  of the hits in the muon chambers with respect to the  
84 linear extrapolation of the tracks from the tracking system. True muons tend to have a  
85 much narrower  $D^2$  distribution, close to zero, than the other particles that are incorrectly  
86 selected by the IsMuon requirement.

87 The average squared distance significance is defined as:

$$D^2 = \frac{1}{N} \sum_i \left\{ \left( \frac{x_{closest}^i - x_{track}^i}{pad_x^i} \right)^2 + \left( \frac{y_{closest}^i - y_{track}^i}{pad_y^i} \right)^2 \right\} \quad (2)$$

88 where the index  $i$  runs over the stations containing hits within the FOI,  $(x_{closest}^i, y_{closest}^i)$   
89 are the coordinates of the closest hit to the track extrapolation point for each station  
90  $(x_{track}^i, y_{track}^i)$  and  $pad_{x,y}^i$  correspond to one half of the pad sizes in the x,y directions.  
91 The total number of stations containing hits within their FOI is denoted by  $N$ .

92 The  $D^2$  distribution for muons depends on the multiple scattering and, therefore, on  
93 the momentum ( $p$ ) and polar angle ( $\theta$ ) distributions of the analyzed sample. In order to  
94 avoid a dependence of the muon likelihood on the calibration sample (with particular  $p$   
95 and  $\theta$ ), the tuning of the muon likelihood is performed separately in momentum bins and  
96 muon detector regions (which correspond to 4 intervals in  $\theta$ ).

97 The likelihood for the non-muon hypothesis is calibrated with the  $D^2$  distribution for  
 98 protons, since the other charged hadrons (pions or kaons) selected by IsMuon will present  
 99 a  $D^2$  distribution with a component identical to the protons and a component very similar  
 100 to the true muons, due to decays in flight before the calorimeter. For protons, the hits  
 101 in the muon system found around the track extrapolation are essentially due to three  
 102 sources: hits from punch-through [13] protons, hits from true muons pointing to the same  
 103 direction of the proton or random hits. The last two are at first order uncorrelated to  
 104 the proton momentum while the first one can present some momentum dependence, less  
 105 important however than the dependence expected for muons. Hence, the tuning of the  
 106 non-muon likelihood is merely performed separately for the 4 muon system regions, due  
 107 to their different granularity.

108 The likelihood for the muon (or non-muon) hypothesis is then defined, for each candi-  
 109 date, as the integral of the calibrated muon (or proton)  $D^2$  probability density function  
 110 from 0 to the measured value,  $D_0^2$ .

111 The results presented in this document are obtained with a muon likelihood calibrated  
 112 with muons from  $J/\psi \rightarrow \mu^+\mu^-$  decays selected from the data taken in 2010, as described  
 113 in Section 4. The non-muon likelihood has been calibrated with a simulated sample of  
 114 decays  $\Lambda^0 \rightarrow p\pi^-$ .

115 The  $D^2$  distributions for muons, protons, pions and kaons obtained from data are  
 116 shown in Fig. 3(a). The distributions of the logarithm of the ratio between the muon  
 117 and non-muon hypotheses (muDLL) are shown in Fig. 3(b). More details about the  
 118 selection of the particles used to make these plots and to extract the performance are  
 119 given in Section 4.

### 120 3.3 Combined likelihoods

121 The muon and non-muon likelihoods presented in Section 3.2 can be combined with the  
 122 likelihoods provided by the RICH systems and the calorimeters to improve the muon  
 123 identification performance.

124 The Cherenkov angles measured in the two RICH detectors are combined with the  
 125 track momentum using an overall event log-likelihood algorithm. For each track in the  
 126 event, a likelihood is assigned to each of the different mass hypotheses (electron, muon,  
 127 pion, kaon and proton). The RICH likelihood can differentiate between muon and other  
 128 particles in particular at low momentum, below 5 GeV/c [14].

129 The energy deposition in the calorimeters also allows the evaluation of likelihoods for  
 130 the muon (minimum ionizing particle), electron and hadron hypotheses.

131 A combined log-likelihood is then obtained for each track and for each of the different  
 132 mass hypotheses by summing the logarithms of the likelihoods obtained using the muon  
 133 system, the RICH and the calorimeters. In this computation, the non-muon likelihood  
 134 obtained in the muon system is assigned to the electron, pion, kaon and proton hypotheses.  
 135 The difference of the combined log-likelihoods for the muon and pion hypotheses (DLL)  
 136 is then used to identify the muons.

137 **3.4 Discriminating variable based on hits sharing**

138 The muon system information is not used in the global track fitting and due to that,  
 139 different tracks can be associated to the same muon hits when the matching of tracks  
 140 to muon chamber hits is performed. Reducing the number of tracks that share hits can  
 141 help to improve the misidentification probability. To use this information, a discriminant  
 142 variable named NShared is built for tracks satisfying the IsMuon criteria and a score of 1  
 143 is added to a given track if it shares hits with another one. The score is given to the track  
 144 to which the hit is more distant. Selecting muon with NShared=0 is a way to reduce the  
 145 probability of incorrectly identifying hadrons as muons. Looser requirements can also be  
 146 applied as shown in Fig. 4.

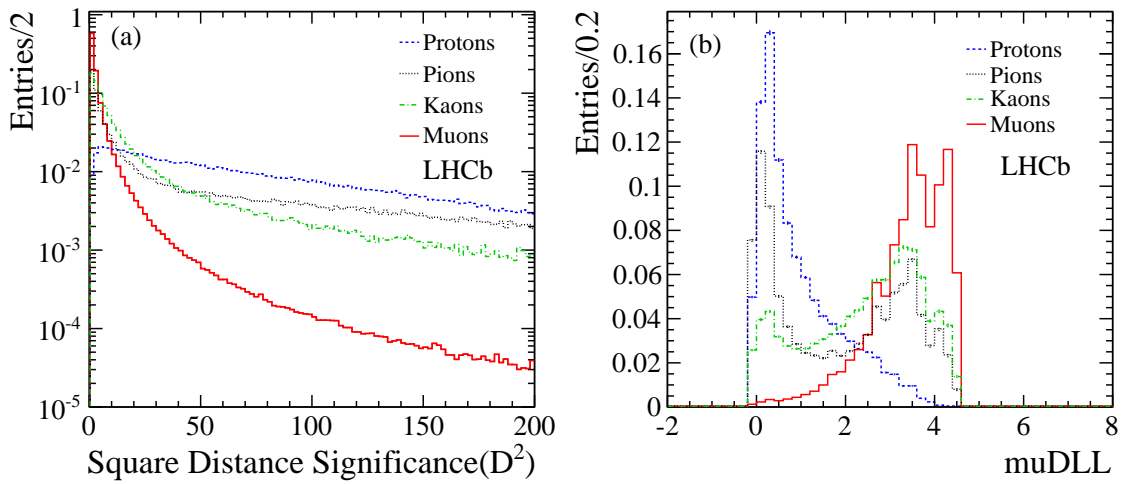


Figure 3: Average square distance significance distributions for muons, protons, pions and kaons (a) and the corresponding muDLL distributions (b).

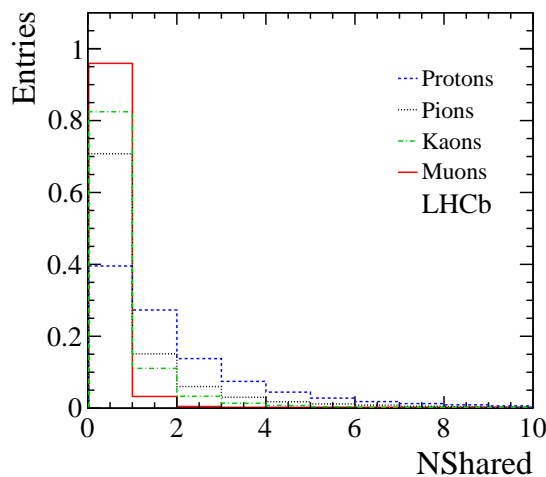


Figure 4: Normalized NShared distributions for muons, protons, kaons and pions.

## 4 Method for the extraction of efficiencies

In order to extract the performance of the muon identification from data, muon, proton, pion, and kaon candidates are selected with high purity from two body decays using kinematical requirements only. When necessary, the purity is improved by using a *tag and probe technique* where particle identification requirements are applied to one of the tracks (tag) while the other (probe) is used for the computation of the muon efficiency or of the hadron misidentification probability.

### 4.1 Selection of control samples

An abundant source of muons is provided in the experiment by the  $J/\psi \rightarrow \mu^+\mu^-$  decay. By requiring the muons to have a high impact parameter with respect to the primary vertex and the reconstructed  $J/\psi$  to have a large flight distance significance and good decay vertex quality, most of the combinatorial background originating from the tracks coming from the primary vertex is removed and the sample gets enriched by  $B \rightarrow J/\psi X$  candidates. In order to reduce further the combinatorial background, one of the muons is required to be identified as a muon. This is defined as the *tag* muon, while the one being probed is only required to have  $p_T > 0.8 \text{ GeV}/c$ .

Protons are selected from the  $\Lambda^0 \rightarrow p\pi^-$  decays reconstructed using decay vertex quality criteria and detachment of the decay vertex from the primary one. Besides, the invariant mass obtained by assigning the  $\pi$  mass to the two daughters is required to be out of a window of  $20 \text{ MeV}/c^2$  around the nominal  $K_s^0$  mass.

The  $D^{*+} \rightarrow \pi^+ D^0$  ( $\rightarrow K^- \pi^+$ ) decays are the source of pions and kaons. Once again relatively high impact parameter is required for the daughters while the  $D^0$  flight direction is required to point to the primary vertex. To evaluate the pion misidentification probability, the tag kaon is selected using a suitable cut on the  $\pi$ - $K$  log-likelihoods difference, based on the RICH information. To evaluate the kaon misidentification probability, the RICH particle identification is used to identify the pion. Quality criteria are used for the  $D^{*+}$  and  $D^0$  decay vertices. A window of  $25 \text{ MeV}/c^2$  around the nominal  $D^0$  mass is used to exclude the doubly Cabibbo suppressed mode and the  $K^+K^-$  and  $\pi^+\pi^-$  decay channels.

To avoid potential biases from the trigger requirements, in the  $J/\psi$  and  $\Lambda^0$  samples only events triggered independently on the probe track are used; this condition has to be satisfied at both hardware and software level, as explained in [15]. For the  $D^0 \rightarrow K^- \pi^+$  sample, a substantial fraction of the events would be lost by such requirement. Therefore the hardware trigger is required to be activated independently on the probe track (kaon or pion) and the software trigger decision is based on impact parameter and detachment from the primary vertex only, with no particle identification requirement.

After the background subtraction of selected two-body decays, the number of muon, proton, pion and kaon candidates in the 2011 data samples are 2.4, 16.1, 11.7 and 12.3 millions, respectively.

## 186 4.2 Efficiency evaluation

As a baseline method to evaluate the efficiency  $\epsilon_{muonID}$  of a generic muon identification requirement denoted in this section by  $muonID$  (e.g. IsMuon true or DLL greater than a given cut), is used :

$$\epsilon_{muonID} = \frac{S_{true}}{S_{true} + S_{false}}, \quad (3)$$

where  $S_{true}$  and  $S_{false}$  are the numbers of signal events satisfying and not satisfying  $muonID$ , extracted from data using

$$S_{true,false} = N_{true,false} - B_{true,false}. \quad (4)$$

187  $N_{true,false}$  are obtained by counting the number of  $J/\psi$  candidates with invariant mass  
 188 lying within a signal mass window around the  $J/\psi$  mass; the number of background  
 189 events within the same mass window,  $B_{true,false}$ , is computed by extrapolating to the  
 190 signal window the mass fit done in the  $J/\psi$  sidebands.

191 For the proton misidentification probability, the same method is used. The kaon  
 192 and pion misidentification probabilities are also obtained with Eq. 3, but  $S_{true,false}$  and  
 193  $B_{true,false}$  are extracted directly from a full fit of the signal and background shapes to the  
 194 invariant mass distribution of the  $D^0$  candidates.

## 195 5 Results

196 The muon identification performance is presented in terms of the muon efficiency and  
 197 hadron misidentification probabilities for the different requirements. In all cases, the  
 198 performance is evaluated for tracks extrapolated within the geometrical acceptance of the  
 199 muon detector.

### 200 5.1 IsMuon performance

201 The efficiency of the IsMuon requirement,  $\epsilon_{IM}$ , is the efficiency of finding hits within  
 202 the fields of interest in the muon chambers for tracks extrapolated to the muon system.  
 203 In Fig. 5,  $\epsilon_{IM}$  is shown as a function of the muon momentum, for different transverse  
 204 momentum ranges. A weak dependency with transverse momentum is observed and in  
 205 particular a drop of  $\sim 2\%$  is measured for the lowest  $p_T$  interval. This efficiency drop is  
 206 essentially due to tracks close to the inner edges of region R1 which in principle have their  
 207 extrapolation points within M1 and M5 acceptance, but are in fact scattered outside the  
 208 detector. For particles with  $p_T$  above 1.7 GeV/c, the efficiency is above 97% in the whole  
 209 momentum range, from 3 GeV/c to 100 GeV/c. The average efficiency obtained for the  
 210  $\mu_{probe}$  in the  $J/\psi$  calibration sample is  $\epsilon_{IM} = (98.13 \pm 0.04)\%$ , for particles with  $p > 3$  GeV  
 211 and  $p_T > 0.8$  GeV/c.

212 The misidentification probabilities  $\wp_{IM}(p \rightarrow \mu)$ ,  $\wp_{IM}(\pi \rightarrow \mu)$  and  $\wp_{IM}(K \rightarrow \mu)$  are  
 213 also shown in Fig. 5. The observed decrease of  $\wp_{IM}$  with increasing transverse momentum

214 is expected, since tracks with higher transverse momentum traverse the detector at higher  
 215 polar angles, in the lower occupancy regions. The proton misidentification probability is  
 216 smaller than 0.5% for all  $p_T$  ranges and momentum above 30 GeV/c. It drops quickly with  
 217 momentum for the lowest  $p_T$  ranges, reaching a plateau at about 30-40 GeV/c. The pion  
 218 and kaon misidentification probabilities have a similar behavior, increasing with decreasing  
 219  $p_T$ . Above 40 GeV/c, the pion misidentification probability is almost at the level of the  
 220 proton misidentification probability. At low momentum, decays in flight are the dominant  
 221 source of incorrect identification, as can be seen from the difference between the pion/kaon  
 222 and proton curves. While the proton misidentification probability, within the  $p_T$  intervals  
 223 chosen, lies within 0.1-1.3%, the pion and kaon misidentification probabilities are within

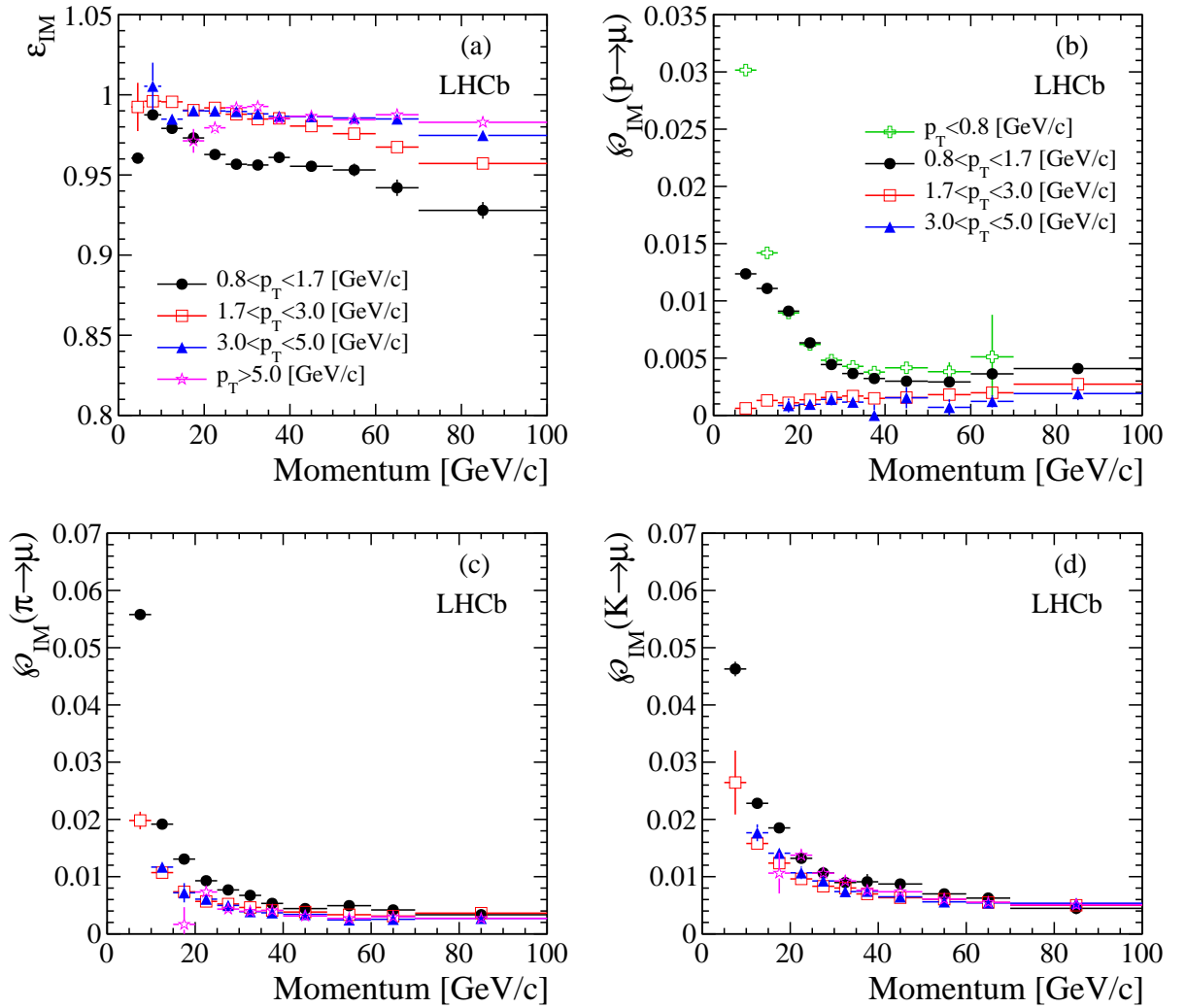


Figure 5: IsMuon efficiency and misidentification probabilities, as a function of momentum, in ranges of transverse momentum:  $\epsilon_{IM}$  (a),  $\phi_{IM}(p \rightarrow \mu)$  (b),  $\phi_{IM}(\pi \rightarrow \mu)$  (c) and  $\phi_{IM}(K \rightarrow \mu)$  (d).

Table 2: Average IsMuon efficiency and misidentification probabilities in different transverse momentum intervals (%).

$p_T$ interval ( GeV/c)	muon	proton	pion	kaon
$p_T < 0.8$		$1.393 \pm 0.005$	$6.2 \pm 0.1$	$4.3 \pm 0.1$
$0.8 < p_T < 1.7$	$96.94 \pm 0.07$	$0.737 \pm 0.003$	$2.19 \pm 0.01$	$1.93 \pm 0.1$
$1.7 < p_T < 3.0$	$98.53 \pm 0.05$	$0.149 \pm 0.004$	$0.61 \pm 0.01$	$0.93 \pm 0.01$
$3.0 < p_T < 5.0$	$98.51 \pm 0.06$	$0.12 \pm 0.02$	$0.40 \pm 0.01$	$0.72 \pm 0.01$
$5.0 < p_T$	$98.51 \pm 0.07$		$0.33 \pm 0.02$	$0.69 \pm 0.01$

224 0.2-5.6% and 0.6-4.5%, respectively. For momentum above 30 GeV/c,  $\wp_{IM}(\pi \rightarrow \mu)$  and  
 225  $\wp_{IM}(K \rightarrow \mu)$  have a small dependence on  $p_T$ . At the lowest  $p_T$  range, the kaon  
 226 misidentification probability is lower than the pion for the lowest momentum interval,  
 227 in spite of the larger decay width of kaons to muons. Since the muon is produced with a  
 228 larger opening angle with respect to the original track trajectory in kaon decays than in  
 229 pion decays, and on average low momentum particles tend to decay further upstream in  
 230 the detector, then the hits in the muon chambers have a higher probability to lie outside  
 231 the fields of interest.

232 When integrated over  $p > 3$  GeV/c and the whole  $p_T$  spectra of our calibration sam-  
 233 ples, the average values for the misidentification probabilities are  $\wp_{IM}(p \rightarrow \mu) = (1.033$   
 234  $\pm 0.003)\%$ ,  $\wp_{IM}(\pi \rightarrow \mu) = (1.025 \pm 0.003)\%$  and  $\wp_{IM}(K \rightarrow \mu) = (1.111 \pm 0.003)\%$ . For pi-  
 235 ons and kaons, about 60% of the misidentification probability is due to decays in flight,  
 236 for these particular samples. The average efficiency and misidentification probabilities,  
 237 integrated over momentum ( $p > 3$  GeV/c), are also given in Table 2, for 5 different  $p_T$   
 238 intervals. There are not enough candidates in the muon, pion and kaon samples for a  
 239 measurement dependent on momentum in the lowest  $p_T$  bin. Similarly for the protons,  
 240 in the highest  $p_T$  interval.

241 The LHCb detector has been designed to operate at the luminosity of  $\mathcal{L} = 2 \times$   
 242  $10^{32} \text{ cm}^{-2} \text{ s}^{-1}$  and with a probability of having one interaction per beam crossing max-  
 243 imal with respect to higher numbers. However, in the 2011 run the experiment operated  
 244 with an average number of interactions per beam crossing about 2.5 times the nominal  
 245 average, with a corresponding increase of the overall detector occupancies. The behavior  
 246 of  $\varepsilon_{IM}$  and  $\wp_{IM}$  was then evaluated as a function of the number of tracks which contain  
 247 hits in the tracking subsystems, from the VELO to the tracking stations. No signifi-  
 248 cant decrease of  $\varepsilon_{IM}$  is observed, while an increase of the misidentification probabilities  
 249 is seen with higher track multiplicities, as expected. The detailed behaviour of both the  
 250 efficiency and the misidentification probabilities as a function of momentum is shown in  
 251 Fig. 6. The probability  $\wp_{IM}(p \rightarrow \mu)$  increases by a factor 2.7 for particles with momentum  
 252 in the range 3 to 5 GeV/c, when comparing events with track multiplicity smaller than 40  
 253 and events with track multiplicity between 150 and 250, which is the highest interval of  
 254 multiplicity analysed. At high momentum, the difference is much less pronounced. For  
 255 pions and kaons, the increase at low momentum is a factor of two, approximately, and

256 drops quickly to a plateau value starting at 20 GeV/c. Since the FOI are smaller at high  
 257 momentum, the misidentification probability becomes less sensitive to the multiplicity of  
 258 the underlying event.

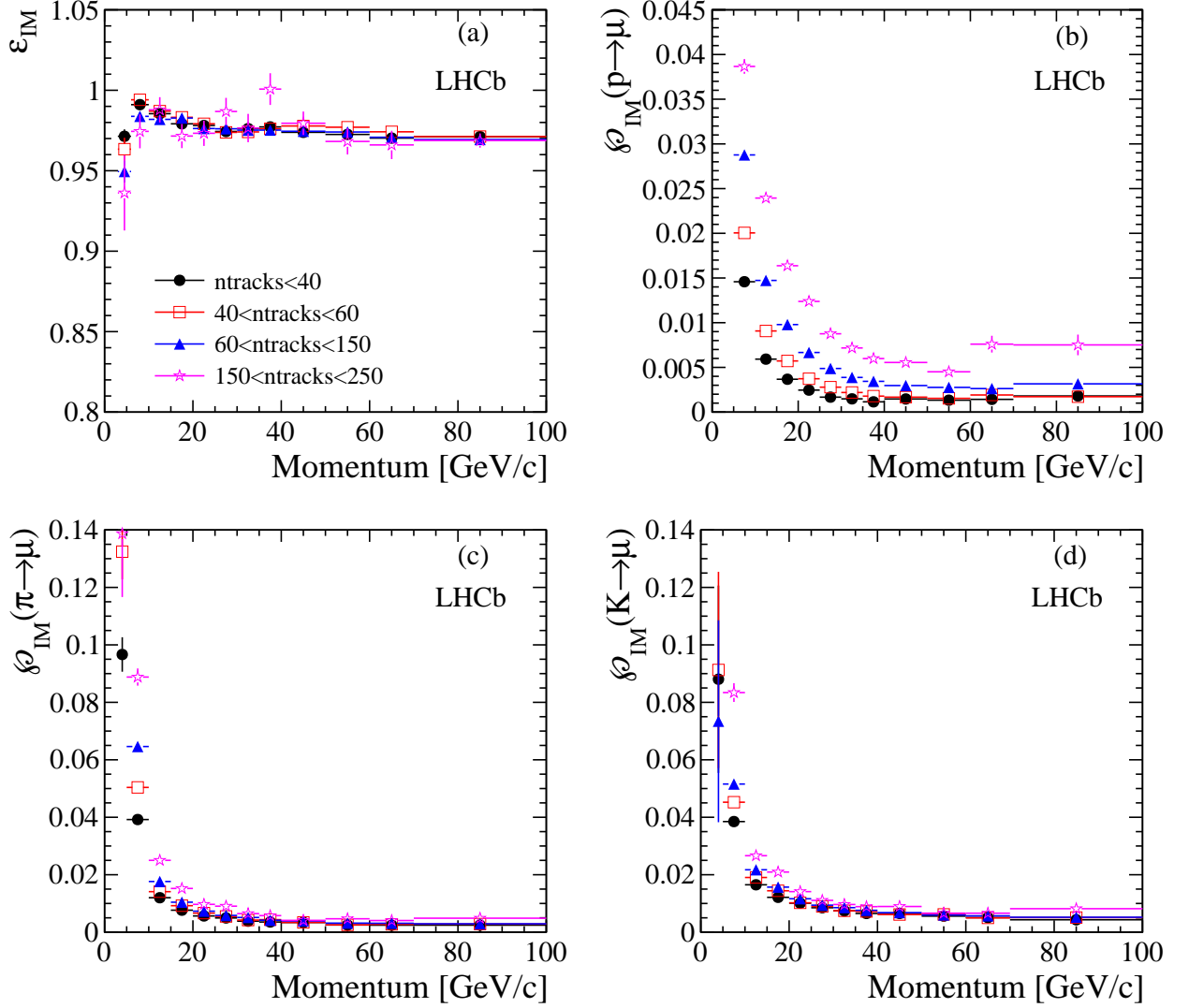


Figure 6: IsMuon efficiency  $\varepsilon_{IM}$  (a) and  $\wp_{IM}$  for protons (b), pions (c) and kaons (d) as a function of momentum for different ranges of the number of trajectories reconstructed in the event ( $n_{tracks}$ ).

259 The charge dependence of the efficiency  $\varepsilon_{IM}$  is also analysed. No difference between  
 260 the efficiencies is seen up to the level of the statistical fluctuations. When integrating over  
 261 the whole momentum range, the relative difference is  $0.09 \pm 0.08\%$ , compatible with zero  
 262 within the statistical uncertainty.

## 5.2 Muon likelihoods

The muon identification efficiency ( $\varepsilon_{\text{muDLL}}$ ) is measured as a function of a selection cut in the variable muDLL, for different momentum ranges, as shown in Fig. 7(a). The misidentification probabilities are also shown in Fig. 7(b) to Fig. 7(d), for the same momentum ranges. The black solid line shows the average fractions, when integrated over  $p > 3 \text{ GeV}/c$  (and  $p_T > 0.8 \text{ GeV}/c$  for the muons). All curves start at the efficiency or misidentification probability corresponding to the IsMuon requirement. For tracks with  $p > 10 \text{ GeV}/c$ , the muon efficiency is independent of momentum up to  $\text{muDLL} \sim 2$ . To achieve a misidentification probability independent from the momentum, the value of the muDLL cut must depend on particle momentum. By applying a muDLL cut irrespective of the momentum, the misidentification probabilities show a strong momentum dependence.

As an example, when requiring  $\text{muDLL} \geq 1.74$ , a cut that provides a final muon efficiency of 93.2%, the final misidentification probabilities are 0.21%, 0.78% and 0.52% for protons, kaons and pions respectively. This cut, which provides a sharp decrease of 5% of the efficiency with respect to the IsMuon efficiency, is used here as an example only for a clear comparison between the muon DLL and the DLL. Since the average efficiency and misidentification probabilities values are given for our calibration samples, which have their particular momentum and  $p_T$  spectrum, they can be different for samples with different kinematic distributions.

The momentum dependence of  $\varepsilon_{\text{muDLL}}$  and of  $\wp_{\text{muDLL}}$  for particles satisfying this cut are shown in Fig. 8, compared to the IsMuon requirement alone and a tighter cut,  $\text{muDLL} \geq 2.25$ . Again, this second cut was chosen for providing a sharp reduction of the muon efficiency of 10% with respect to the IsMuon efficiency. Once more, since the performance is integrated over  $p_T$ , small variations from these values are expected for different samples, in particular for the misidentification probabilities, which present a stronger dependence with transverse momentum.

## 5.3 Combined likelihoods

The DLL efficiency is shown as a function of the pion and kaon misidentification probabilities in Fig. 9, together with the results obtained using the muDLL alone, allowing for a direct comparison of their performances.

The DLL benefits from RICH and calorimeter information, being more effective than the muon DLL alone in separating pions and kaons from muons. After IsMuon, this is the most used particle identification requirement used to select muons in LHCb and the actual cut value is usually chosen according to the compromise between purity and efficiency needed for that specific study. The average misidentification rates corresponding to a cut which provides an average decrease of 5% (equivalent to the one obtained with  $\text{muDLL} \geq 1.74$ , as previously shown) are around 0.65% and 0.38% for the kaons and pions, respectively.

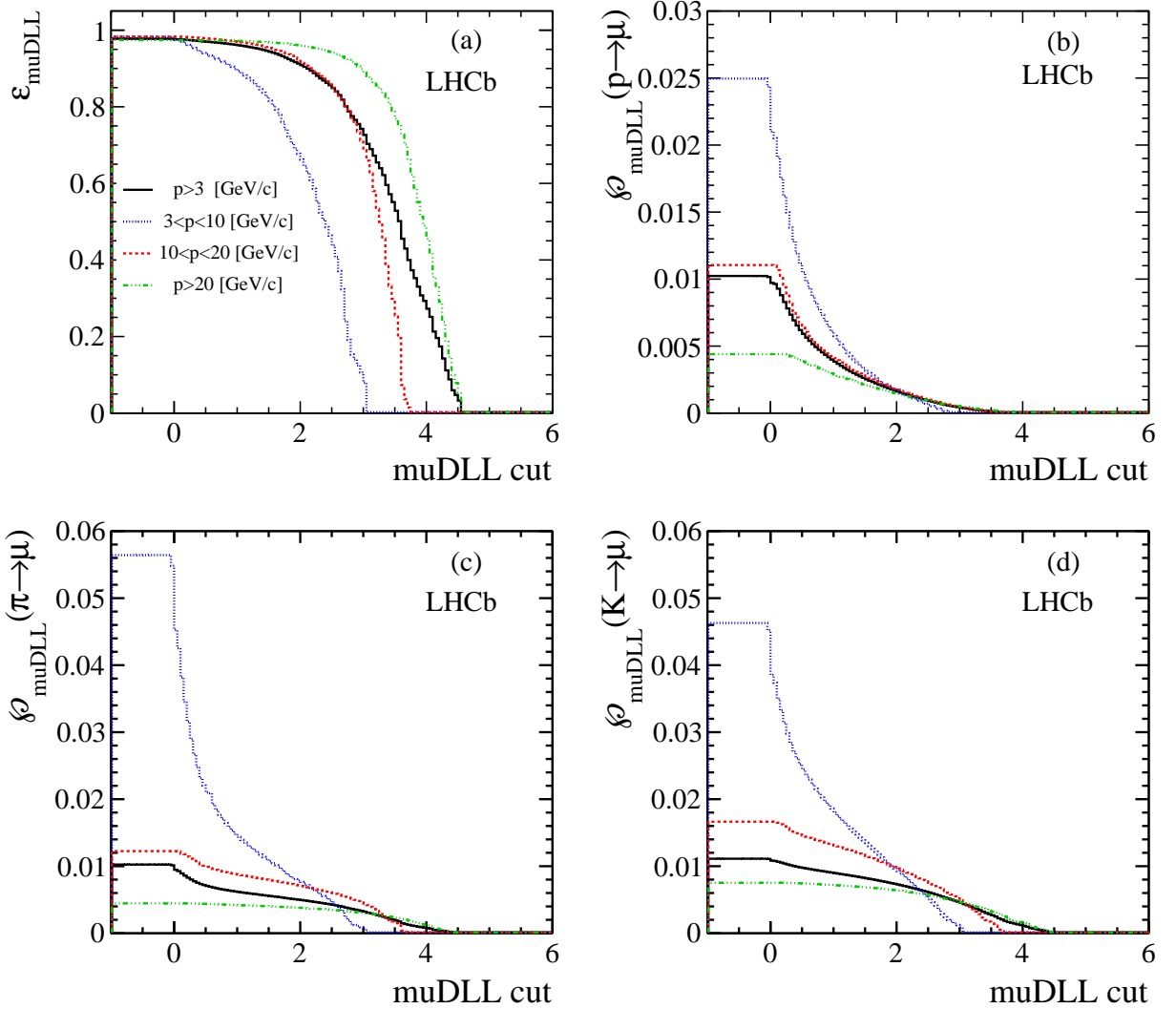


Figure 7: The efficiency  $\varepsilon_{\text{muDLL}}$  as a function of muon DLL cut for muons (a) and misidentification probabilities for protons (b), pions (c) and kaons (d). The black solid line shows the average values integrated over  $p > 3 \text{ GeV}/c$ . The blue dotted line correspond to particles in the range  $3 < p < 10 \text{ GeV}/c$ . The red dashed lines show results for  $10 < p < 20 \text{ GeV}/c$  and the green dashed-dotted for  $p > 20 \text{ GeV}/c$ .

## 302 5.4 NShared performance

303 As mentioned in Section 3, after requiring IsMuon, an additional way of reducing the  
 304 incorrect identification probability of hadrons as muons, in particular at high occupancy,  
 305 is the use of a cut on NShared.

306 The muon efficiency is shown as a function of the pion misidentification probability  
 307 for corresponding NShared cut in Fig. 10(a); protons are shown in Fig. 10(b). Due to  
 308 similar decay-in-flight pollution at low momentum, kaons behave as pions. The black

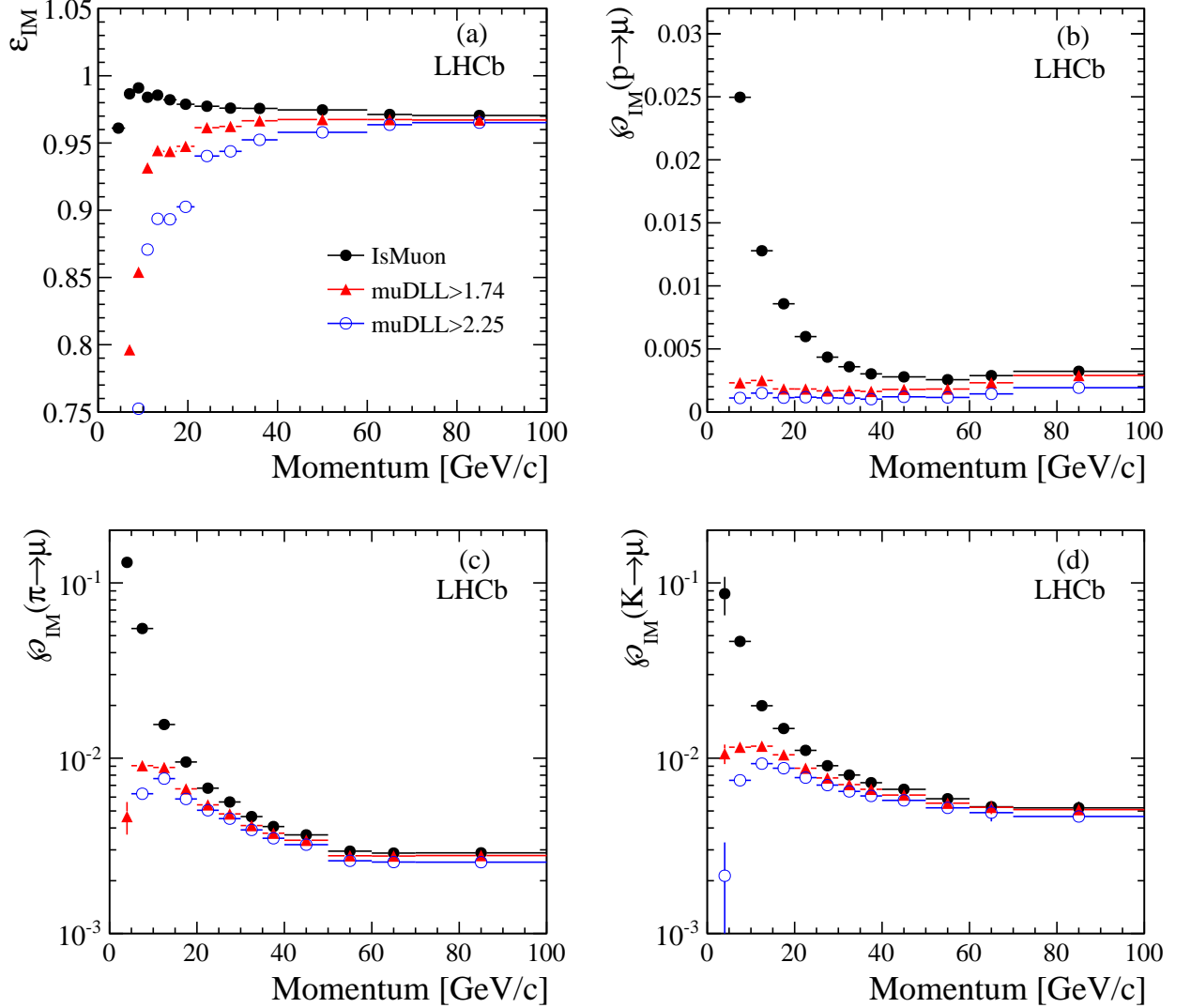


Figure 8: Muon efficiency (a) and misidentification probabilities for protons (b), pions (c) and kaons (d) as a function of the particle momentum for the IsMuon requirement alone (black solid circles) and with the additional cuts  $\text{muDLL} \geq 1.74$  (red triangles) and  $\text{muDLL} \geq 2.25$  (blue open circles).

309 solid line shows the average values integrated over  $p > 3 \text{ GeV}/c$ . The NShared selection  
 310 is particularly effective at low momenta, with increasing the FOI size.

## 311 5.5 Systematic checks

312 The effect of the trigger and of the method chosen to evaluate the efficiency and  
 313 misidentification probabilities are investigated.

314 Alternatively to the requirement of the  $J/\psi \rightarrow \mu^+ \mu^-$  sample being triggered indepen-

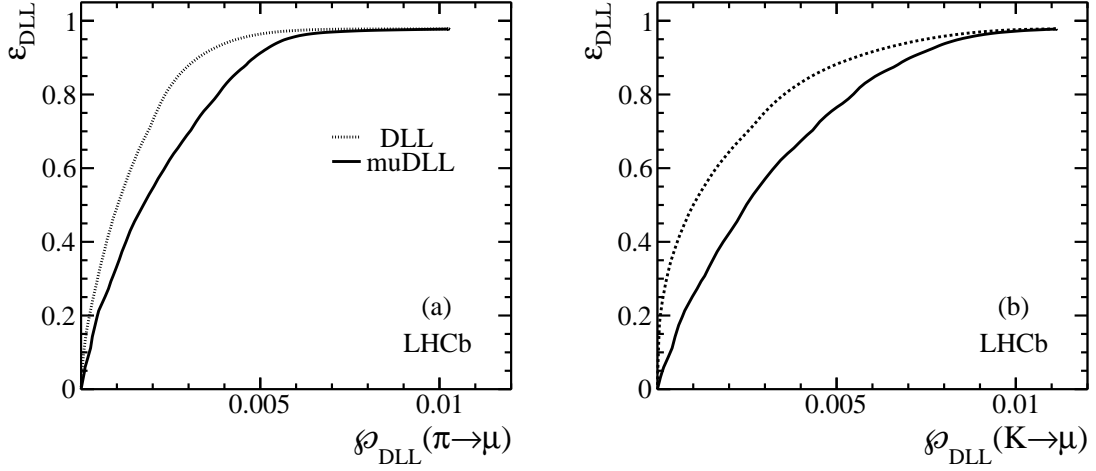


Figure 9: Average efficiency  $\varepsilon_{\text{DLL}}$  as a function of the pion (a) and kaon (b) misidentification probabilities for particles with momentum in the range  $p > 3 \text{ GeV}/c$ . The dotted lines show the DLL performance, while the muon DLL performance is shown with a solid line.

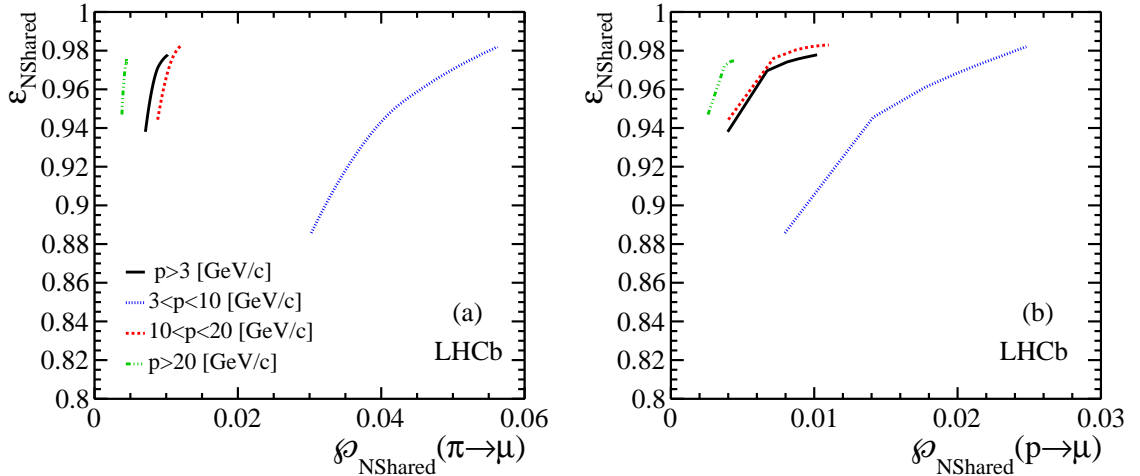


Figure 10: Muon efficiency  $\varepsilon_{\text{NShared}}$  as a function of the pion and proton misidentification probabilities. The average values, for all particles with  $p > 3 \text{ GeV}/c$ , are shown with a black line, compared to the three momentum ranges separately, as for Fig. 7.

315 dently of the probe muon, a muon trigger decision based on the tag muon was used to  
 316 evaluate the IsMuon efficiency. The systematic uncertainty due to the choice of trigger  
 317 strategy is taken as the difference between the two determinations, which is 0.2%.

318 When performing a full fit to the signal and background components of the mass  
 319 distributions used to extract the yields of signal events satisfying or not the muon iden-

320 tification requirements, the resulting efficiencies and proton misidentification probability  
321 rates agree within the statistical uncertainties with the results shown in Section 5.

322 For the pion and kaon misidentification probabilities, the effect of the trigger is studied  
323 and found to be negligible within the uncertainties, independently of momentum and  
324 transverse momentum. Also the systematic uncertainty related to the method used for  
325 the evaluation of the efficiency is found to be negligible as a function of momentum, apart  
326 from a few intervals where it is comparable with the statistical accuracy.

## 327 **6 Conclusions**

328 The performance of the muon identification procedure used in the LHCb experiment has  
329 been evaluated, using a dataset corresponding to  $1 \text{ fb}^{-1}$  recorded in 2011 at  $\sqrt{s} = 7 \text{ TeV}$ .

330 A loose binary criterium that can be used to select muons is based on the matching  
331 of muon hits with the particle trajectory. For candidates satisfying this requirement,  
332 likelihoods for muon and non-muon hypotheses are built with the pattern of hits around  
333 the trajectories, which can be used to refine the selection. An additional way of rejecting  
334 fake muon candidates is provided by a variable sensitive to hit sharing by nearby particles.

335 The muon identification efficiency was observed to be robust against the variation  
336 of detector occupancies and presents a weak dependence on momentum and transverse  
337 momentum. Hadron misidentification probabilities present a stronger dependence on hit  
338 or track multiplicity, however the highest increase factors are observed only for low mo-  
339 mentum particles.

340 Average muon identification efficiencies at the 98% level are attainable for pion and  
341 kaon misidentification below the 1% level at high transverse momentum, using the loosest  
342 identification criterium. The performance of additional requirements based on likelihoods  
343 or on hits sharing can be tuned according to the needs of each analysis and reduce the  
344 misidentification probabilities dependence on track multiplicity. Adding a requirement on  
345 the difference of the log-likelihoods that provides a total muon efficiency at the level of  
346 93%, the hadron misidentification probabilities are below 0.6%.

## 347 **Acknowledgements**

348 We express our gratitude to our colleagues in the CERN accelerator departments for  
349 the excellent performance of the LHC. We thank the technical and administrative staff at  
350 CERN and at the LHCb institutes, and acknowledge support from the National Agencies:  
351 CAPES, CNPq, FAPERJ and FINEP (Brazil); CERN; NSFC (China); CNRS/IN2P3  
352 (France); BMBF, DFG, HGF and MPG (Germany); SFI (Ireland); INFN (Italy); FOM  
353 and NWO (The Netherlands); SCSR (Poland); ANCS (Romania); MinES of Russia and  
354 Rosatom (Russia); MICINN, XuntaGal and GENCAT (Spain); SNSF and SER (Switzer-  
355 land); NAS Ukraine (Ukraine); STFC (United Kingdom); NSF (USA). We also acknowl-  
356 edge the support received from the ERC under FP7 and the Region Auvergne.

## References

- [1] LHCb collaboration, A. A. Alves Jr. *et al.*, *The LHCb detector at the LHC*, JINST **3** (2008) S08005.
- [2] LHCb collaboration, R. Aaij *et al.*, *Strong constraints on the rare decays  $B_s^0 \rightarrow \mu^+ \mu^-$  and  $B_d^0 \rightarrow \mu^+ \mu^-$* , Phys. Rev. Lett. **108** (2012) 231801, arXiv:1203.4493.
- [3] LHCb collaboration, R. Aaij *et al.*, *First observation of the decay  $B^+ \rightarrow \pi^+ \mu^+ \mu^-$* , J. High Energy Phys. **12** (2012) 125, 1210.2645.
- [4] LHCb collaboration, R. Aaij *et al.*, *Measurement of the isospin asymmetry in  $B \rightarrow K^{(*)} \mu^+ \mu^-$  decays*, J. High Energy Phys. **07** (2012) 133, 1205.3422.
- [5] LHCb collaboration, R. Aaij *et al.*, *Differential branching fraction and angular analysis of the decay  $B^0 \rightarrow K^{*0} \mu^+ \mu^-$* , Phys. Rev. Lett. **108** (2011) 181806, arXiv:1112.3515.
- [6] LHCb collaboration, R. Aaij *et al.*, *Search for the lepton number violating decays  $B^+ \rightarrow \pi^- \mu^+ \mu^+$  and  $B^+ \rightarrow K^- \mu^+ \mu^+$* , Phys. Rev. Lett. **108** (2011) 101601, arXiv:1110.0730.
- [7] LHCb collaboration, R. Aaij *et al.*, *Measurement of the  $B_s^0 \rightarrow J/\psi \bar{K}^{*0}$  branching fraction and angular amplitudes*, Phys. Rev. D **86** (2012) 071102, arXiv:1208.0738.
- [8] LHCb collaboration, R. Aaij *et al.*, *Measurement of the  $cp$ -violating phase  $\phi_s$  in the decay  $B_s^0 \rightarrow J/\psi \phi$* , Phys. Rev. Lett. **108** (2011) 101803, 1112.3183.
- [9] LHCb collaboration, R. Aaij *et al.*, *Measurement of the  $cp$  violating phase  $\phi_s$  in  $\bar{B}_s^0 \rightarrow J/\psi f_0(980)$* , Phys. Lett. B **707** (2011) 497505, 1112.3056.
- [10] A. A. Alves Jr. *et al.*, *Performance of the LHCb muon system*, JINST **8** (2013) P02022, arXiv:1112.1346.
- [11] R. Aaij and J. Albrecht, *Muon triggers in the High Level Trigger of LHCb*, LHCb-PUB-2011-017 (2011).
- [12] M. Clemencic *et al.*, *The LHCb simulation application, GAUSS: design, evolution and experience*, J. Phys: Conf. Ser. **331** (2011) 032023.
- [13] C. Grupen, *Particle Detectors*. Cambridge university press, Cambridge, England, 1996.
- [14] M. Adinolfi *et al.*, *Performance of the LHCb RICH detector at the LHC*, arXiv:1211.6759.
- [15] R. Aaij *et al.*, *The LHCb Trigger and its Performance*, arXiv:1211.3055.